

Shock-compaction features and shock-induced chemical reaction in some ceramic powders

K. KONDO, S. SOGA, E. RAPOPORT*, A. SAWAOKA

*Research Laboratory of Engineering Materials, Tokyo University of Technology,
4259 Nagatsuta, Midori, Yokohama 227, Japan*

M. ARAKI

Nippon Oil and Fats Co, Ltd, Aza-Nishimon, Taketoyo, Chita, Aichi 470-23, Japan

Shock compaction features are experimentally investigated for some selected ceramic materials and ceramic composite systems, i.e. SiC, AlN, SiC/AlN, and AlN/Al₂O₃. A typical microstructure to support the skin model proposed in a previous paper is obtained by using SiC powder with a particle diameter of several micrometres. AlN transforms into an unknown phase. The transformation needs a small amount of oxygen. The amount of the unknown new phase decreases with the increase of shock temperature. Chemical reaction of AlN/Al₂O₃ mixture into ALON (cubic aluminium oxynitride spinel) occurs under shock loading and proceeds along with increasing shock temperature. Crystallite size and microstrain of the samples are determined by X-ray line broadening analysis. The microstrain for mixture sample and fine powder is larger than that for single-component sample and coarse powder, respectively. As suggested by the skin model, the requirement that the initial particle size is less than 1 μm is essential for ceramic powder to be consolidated by a shock compaction technique in order to yield good compacts of optimum strength and to achieve chemical reaction accompanying mass transport.

1. Introduction

A shock processing, which utilizes both disruptive forces within a shock front and bonding effects due to high stresses and high temperatures in a shock wave, can offer many potential advantages in powder consolidation, conditioning of metal and ceramic powders, and synthesis of new materials. Some of these advantages in the process provide densities approaching theoretical in a wide variety of difficult-to-compact metals and ceramics with unique and often nonequilibrium microstructures, which may produce unique properties, unexpected desirable features, and so on [1, 2]. Although the shock processing is rather simple in practice, phenomena occurring upon the process are extremely complicated, consisting of many factors such as shape and size of particle, their distribution, physical and chemical properties of materials, porosity, and system parameters (shock pressure, attenuation, and shock temperature, as well as shock-wave geometry). Therefore, concerning the process, systematic studies are required in order to make the shock processing applicable to industrial production.

The shock processing, especially shock compaction of powders, must precisely control the heterogeneous state of powder aggregate which is realized in and behind a shock-wave front by shock wave passage. In the previous paper on shock compaction of SiC powder, the skin model for analysing the heterogeneous shock state has been proposed [2]. The skin model enables one to estimate heterogeneous temperature

distribution and the subsequent thermal relaxation phenomena. The model suggests that the thermal relaxation phenomena become critical for the grain size of a few micrometres in the ceramic compact under and after shock loading [2]. The heterogeneous shock state in the powder aggregate caused by shock compression will be more remarkable in a multiphase or composite system than other simple systems. We suppose that the shock compaction of the composite system will enable the avoidance of one of the principal shortcomings of shock compaction, namely cracking, and to produce excellent and unique engineering materials. Conversely, shock compaction experiments for such a system will become an effective way to investigate the shock-induced heterogeneous state. For instance, a composite system consisting of materials with different melting temperatures would respond to the heterogeneous temperature distribution which may promote chemical reaction among different kinds of atoms. When a material in the composite system is melted, its chemical reactivity will remarkably increase and become much greater than that in the solid state reaction. For the application of shock-compression techniques to material processing, it is also important to study the chemical reaction during shock compaction, because it is not well-known how mass transport occurs in such a short time as this kind of shock loading. These studies will also make it clear how the shock processing is influenced by impurities.

Present address: Israel Atomic Energy Commission, Soreq Nuclear Research Centre, Yavne 70600, Israel.

In this paper, we describe preliminary experiments on shock-compaction features of some selected ceramic materials and ceramic composite systems. Silicon carbide (β -SiC) powder with larger particle sizes than in the previous experiments [2] is used to investigate a grain-size effect in shock-compaction phenomena. Aluminium nitride (AlN) powder is investigated because of its different mechanical and thermal properties from SiC. It is also suggested that the material has two kinds of phase transition under high pressure [3, 4]. Mixtures of SiC and AlN powders with 50/50 mole ratio and of AlN and Al_2O_3 powders with 36/64 are used to investigate shock-compaction features of ceramic composite systems and chemical reaction phenomena accompanying mass transport.

2. Experimental techniques

SiC powder used as a starting material was of stock commercial grade, Betarundum as a trade name, which was supplied by Ibiden Co, Ltd (Ogaki, Japan). The powder has cubic structure, β -SiC. The average size and the purity of the powder are $5.3\ \mu\text{m}$ and 99.4%, respectively. AlN powder with 98% purity (the major impurity was oxygen of about 1.26 mass %) and 3 to $5\ \mu\text{m}$ particle size was supplied by Toshiba Ceramic Co, Ltd. Another AlN powder with 99% purity and with $2\ \mu\text{m}$ particle size was used for comparison experiments. The high-purity AlN powder was provided by High Purity Chemical Laboratory, Inc. Al_2O_3 powder was of stock commercial grade with

nominal particle size of $0.3\ \mu\text{m}$, supplied by Meller Co, Ltd, USA. Mixtures of SiC/AlN powder with 50/50 mole ratio and of AlN/ Al_2O_3 powder with 36/64 mole ratio were prepared by using a resin-lined ball mill for 12 h. The mixtures were heat-treated at 500°C for 1 h in order to remove the resin. Scanning electron micrographs for the starting powders are shown in Fig. 1.

These powders were packed into a stainless steel capsule. The capsule was in the shape of a column 30 mm length and 24 mm diameter with a small hole allowing the evacuation of air from the inside of the capsule before tightening a plug. The sample space in the capsule was 12 mm diameter and 5 mm high. Both the amount of powder charged and the packing pressure used were varied so as to obtain the porosity required.

Experimental procedures of shock compression were similar to those described earlier [2]. Four capsules with different densities of sample were set in a momentum-trap assembly and simultaneously impacted by an explosively driven flyer plate of iron, 3.2 mm thick, where a mouse-trap type plane-wave generator was used [2]. The momentum-trap assembly, consisting of three pieces of iron ring and plates, was 120 mm diameter and 60 mm high. Impact velocities of the flyer were 2, 2.3 and $3\ \text{km}\ \text{sec}^{-1}$, to which the generated shock pressures of 45, 54 and 77 GPa for the capsule material of SUS 304 stainless steel corresponded, respectively. Pressures in the samples were different from these capsule pressures, as described

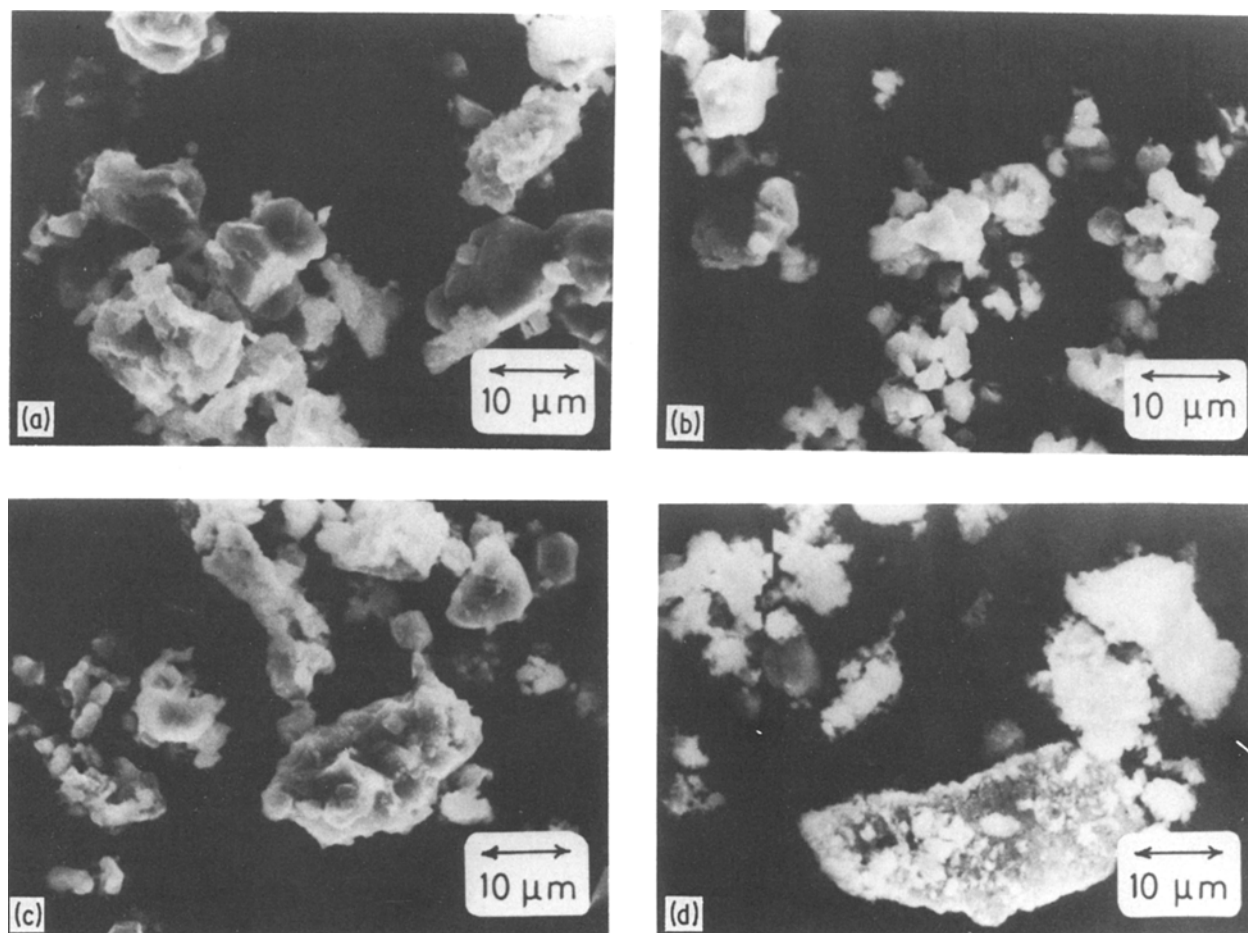


Figure 1 Scanning electron micrographs of starting powders (a) SiC, (b) SiC/AlN with 50/50 mole ratio, (c) AlN, (d) AlN/ Al_2O_3 with 36/64 mole ratio.

TABLE I Summary of experimental conditions and results

Sample number	Material	Initial density (%)	Flyer velocity (km sec ⁻¹)	Shock pressure (GPa)	Shock temperature (K)	Relative density (%)	Vickers hardness (kg mm ⁻²)
1-1	SiC	65	2.0	13.4	1430	—	—
1-2	SiC/AlN	65	2.0	—	—	93.5	—
1-3	AlN	65	2.0	—	—	93.7	1240
1-4	AlN/Al ₂ O ₃	65	2.0	—	—	—	—
2-1	SiC	50	2.3	11.3	1950	96.3	1740
2-2	SiC/AlN	50	2.3	—	—	94.2	1440
2-3	AlN	50	2.3	—	—	94.2	1410
2-4	AlN/Al ₂ O ₃	50	2.3	—	—	94.1	820
3-1	SiC	35	3.0	10.3	3270	—	—
3-2	SiC/AlN	35	3.0	—	—	—	—
3-3	AlN	35	3.0	—	—	94.5	—
3-4	AlN/Al ₂ O ₃	35	3.0	—	—	—	—
4-3	AlN*	99	3.0	50 [†]	—	—	—
5-3	AlN*	71	3.0	30 [†]	—	—	—

*High purity material.

[†]Roughly estimated from the data [3].

later. After impact, everything was driven into a water basin and then recovered from the water.

The experimental conditions employed here are summarized in Table I.

Subsequent to the shock treatment, samples were recovered by shaving off the capsule material carefully with a lathe. Apparent density and Vicker's microhardness for some shock-compacted samples were measured. Fracture surfaces of all the samples recovered were observed by a scanning electron microscope. X-ray diffraction experiments on the sample crushed by an agate mortar were carried out to obtain lattice parameters, microstrain, and a crystallite size by using the Hall equation [5–7].

Although it is possible to estimate the shock state, i.e. pressure and temperature, in a mixture of powders or composite under shock loading [8, 9], the estimated values have never been demonstrated experimentally. The estimation procedure requires various types of assumptions. Moreover, the Hugoniot compression data available for AlN are of a preliminary nature and not precise enough [3]. Therefore, we have not estimated the shock state in the SiC samples only. Because the physical properties of AlN and Al₂O₃ resemble those of SiC, the shock pressure and shock temperature are not so different from those in SiC samples under the assumptions of no phase change and the equilibrium to be achievable. The shock state in SiC samples is estimated via a similar method to the previous one [2], and summarized in Table I. It can be seen in this series of experiments that shock temperature increases with the increase of impact velocity of the flyer under approximately constant pressure conditions, as shown in Table I.

3. Results

3.1. Appearance

Relative density and the Vicker's microhardness for several shock-compacted samples are listed in Table I. All the densities for the samples measured exceed 93%. Those for the other samples were difficult to measure, because they could not be recovered as integral samples. Only a small amount of AlN/Al₂O₃

powder which was shock loaded at 3 km sec⁻¹ was recovered because of a breakage of the capsule. The relative density for the sample of SiC (2-1), which was of 50% initial density and was impacted at a velocity of 2.3 km sec⁻¹, is slightly higher than that of the previous fine powder experiments. The Vicker's microhardness for SiC is considerably lower than both the previous data (2600 to 2700 kg m⁻²) [2] and those in statically sintered SiC, but the hardness for AlN is comparable to other published values of statically sintered AlN [10, 11].

3.2. X-ray analysis

The crystal structure of the shock-compacted SiC and SiC/AlN samples, which was determined by a powder X-ray diffraction technique, does not show any change from the starting material, as shown in Fig. 2. On the other hand, AlN and AlN/Al₂O₃ samples show new peaks on the X-ray diffraction pattern, as shown in Figs. 3 and 4, respectively. The unidentified peaks for the AlN sample fairly correspond to the new phase synthesized by both shock and static compression techniques, which were reported by Vereshchagin *et al.* [4]. These peaks appear on the diffraction pattern for AlN/Al₂O₃ mixture (Fig. 4) but not for the SiC/AlN (Fig. 2). The proportion of the new phase of AlN decreases with the increase of impact velocity in both of the systems of single-component AlN and AlN/Al₂O₃ mixture. The peaks do not appear on the diffraction pattern for high-purity AlN, where the shock pressure is much higher than in the other experiments and exceeds the phase transition pressure from wurtzite structure to sodium chloride structure [3]. It is clear from Figs. 2, 3 and 4 that the new phase creation is strongly influenced by both the magnitude of impact velocity and the oxidizing atmosphere. The amount of the new phase of AlN produced at an impact velocity of 2 km sec⁻¹ in the AlN/Al₂O₃ samples is four times larger than that in the single-component AlN sample, as deduced from the strongest peak of AlN.

The X-ray diffraction pattern for the AlN/Al₂O₃ mixture shows other additional peaks. They can be

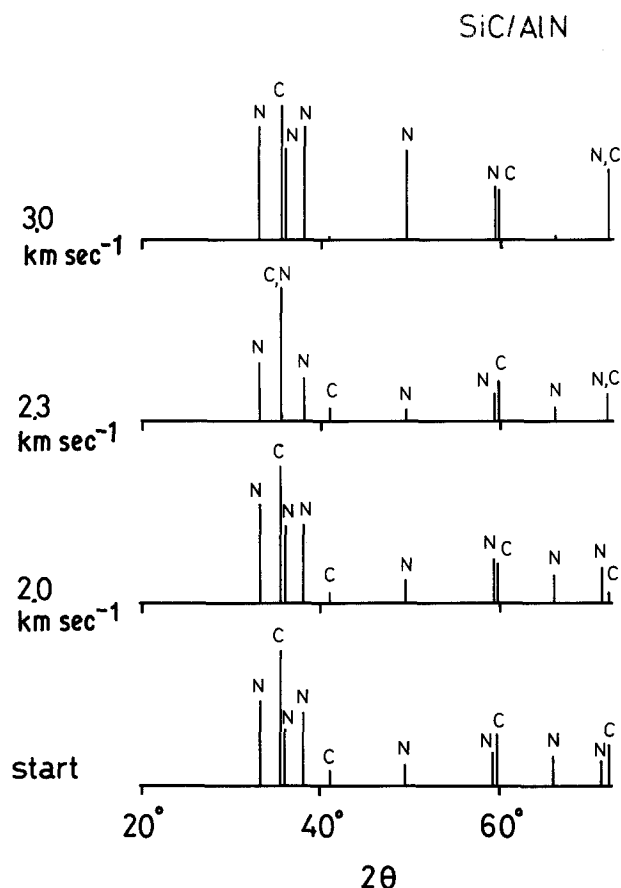


Figure 2 Changes in X-ray diffraction patterns for SiC/AlN sample with 50/50 mole ratio, obtained by nickel filtered X-rays from a copper target. C and N denote SiC and AlN peaks, respectively.

identified as cubic aluminium oxynitride spinel ($5\text{AlN} \cdot 9\text{Al}_2\text{O}_3$, ALON) [12–14]. It can be seen from Fig. 4 that the amount of ALON increases with the increase of impact velocity. This shows that the chemical reaction of AlN and Al_2O_3 for ALON reasonably depends on the average shock-temperature. The formation of ALON is evidence that reconstructive chemical reaction occurs in such a short time duration under shock loading.

Since all the X-ray diffraction patterns except for Al_2O_3 of sample 3-4 are broadened, it suggests that the crystals of every material are deformed and are pulverized, as similar to the other shocked ceramic materials [1, 2, 7, 15–17]. Crystallite size and microstrain of the samples were determined by X-ray line broadening analysis by use of the Hall equation and the Rachinger's correction method [5, 6]. Table II summarizes results of the analysis. For the single-component SiC sample, slight crystallite size reduction occurs due to shock loading, but the remarkable increase of microstrain is observed at an impact velocity of 2 km sec^{-1} . The microstrain slightly decreases with the increase in impact velocity. At an impact velocity of 3 km sec^{-1} , the result for the SiC sample shows annealing effects, which means both an increase of crystallite size and a decrease of microstrain, but shock disruptive effects still remain for SiC crystal in SiC/AlN mixture at that velocity.

On the other hand, the general tendency of the shock disruptive effects for AlN is similar to that for SiC, but the maximum effects appear at an impact

velocity of 2.3 km sec^{-1} . The effect of crystallite size reduction for AlN is smaller than that of SiC, but the remarkable increase of microstrain is observed for AlN in SiC/AlN and AlN/ Al_2O_3 mixtures. This remarkable increase of microstrain remains even at an impact velocity of 3 km sec^{-1} , conversely in the case of SiC. The increase of microstrain in the case of the mixture is affected by chemical reaction between the sample materials which have a different crystal structure. The large microstrain increase for the high-purity AlN sample which was impacted at 3 km sec^{-1} (samples 4-3 and 5-3) is caused by the phase transition from wurtzite structure to sodium chloride structure. The shock disruptive effects for Al_2O_3 are not clear. At an impact velocity of 3 km sec^{-1} , the annealing effects are remarkable, though Al_2O_3 crystals are in the AlN/ Al_2O_3 mixture.

3.3. SEM observations

3.3.1. SiC

Fig. 5 shows scanning electron micrographs of fracture surfaces of the SiC samples. As seen in Fig. 5a, the microstructure suggests a wide range of particle-size distribution. The microstructure is quite different from those shown in the photographs of the fine particle experiments [2]. This difference is consistent with the similar results for Al_2O_3 shock compaction experiments reported by Prümmer and Ziegler [16] who determined the effects of particle size by using fine ($3 \mu\text{m}$) and course ($300 \mu\text{m}$) powders. It is clear that the small particles are fragments which are produced by pulverization due to collision and friction among the particles. Since the small fragments of SiC

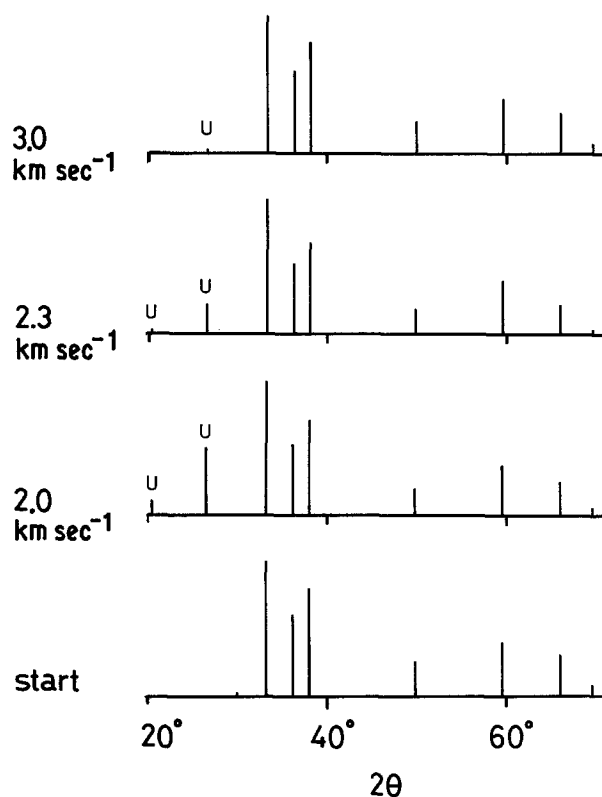


Figure 3 Changes in X-ray diffraction patterns for AlN single sample obtained by nickel filtered X-rays from a copper target. U denotes an unknown new phase, and the other peaks correspond to the starting powders.

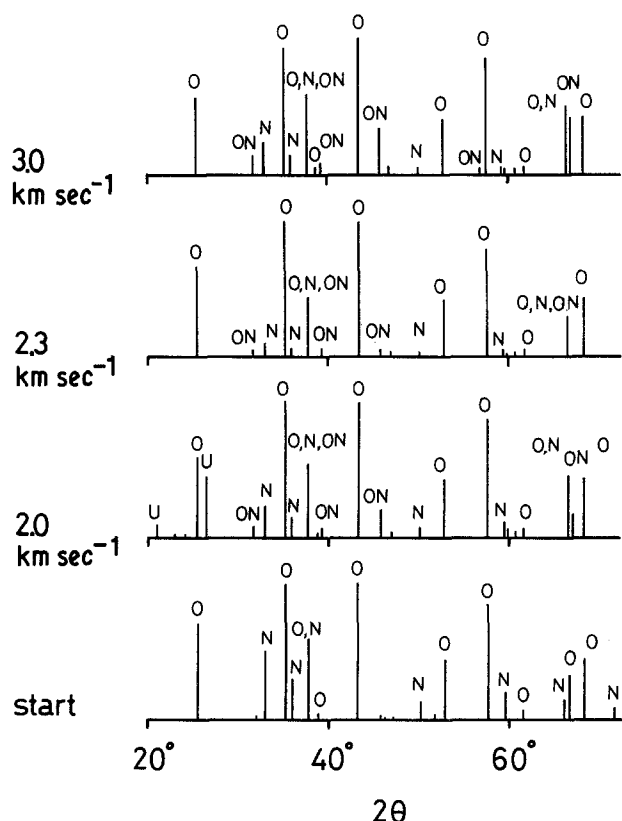


Figure 4 Changes in X-ray diffraction patterns for AlN/Al₂O₃ with 36/40 mole ratio, obtained by nickel filtered X-rays from a copper target. N, U, O and ON denote AlN, new unknown phase of AlN, α -Al₂O₃ and ALON, respectively.

particles fill pores, the relative density of the compact seems considerably increased. However, this sample, which was impacted at a flyer velocity of 2 km sec⁻¹, was not obtained as a firm compact. The reason is that many cracks exist both in a large particle and at the interface between the large particle and the matrix consisting of the fragments. Moreover, bonding among particles seems to be incomplete and weak, because we can see many voids, which are traces of particles removed without difficulty.

At a 2.3 km sec⁻¹ impaction, small fragments melt, join each other, and form a continuous matrix, as shown in Fig. 5b. The corners of a large particle are rounded, and the large particles are also joined to each other by the matrix. With this microstructure, it is reasonable to obtain a higher relative density, and it is similar to the results of Prümmer and Ziegler for Al₂O₃ powder. Obviously, this phenomenon is caused

by the thermal energy increase which corresponds to the average temperature increase of approximately 500°C. However, the large particles probably include many microcracks because the Vicker's microhardness for this sample is lower than the previous shock-compaction data for fine SiC powder.

Fig. 5c shows that recrystallization and crystal growth occur and form a twinned crystal shaped like a macle of natural diamond crystal, which is well developed in the (1 1 1) crystallographic plane. Fig. 5c resembles quite well the previous photograph for SiC fine particles (0.3 μ m) experiments, where the size of the particles or the twinned crystals is 1 to 3 μ m. In contrast with this, the recrystallized particle size is approximately 10 μ m for the larger particle size SiC used here. In Fig. 5c we can see small free spheres and adhered matter which are caused by the fact that the small fragments melt. They serve as a material source for the recrystallization. The mechanism for the recrystallization is an epitaxial growth from the liquid phase. Since the shock conditions, except for the initial particle size, were almost the same in both the experiments, the difference between the recrystallized particle sizes is dependent solely on the initial particle size or the number of initial particles. It is, therefore, likely that heterogenous nucleation occurs in the large particle like those in Fig. 5a because of the heterogeneous temperature distribution mentioned in the skin model [2].

3.3.2. SiC/AlN

Fig. 6 shows scanning electron micrographs for fracture surfaces of the SiC/AlN mixture samples. At a 2 km sec⁻¹ impaction, a photograph similar to the single-component SiC sample impacted at a velocity of 2 km sec⁻¹ is obtained as shown in Fig. 6a. Large particles in the photograph are probably of SiC. Independent small fragments are less than those in SiC, and a relatively continuous matrix is formed. The other features, for example cracks, are considerably similar to those for SiC. Fig. 6b is for the sample impacted at a velocity of 2.3 km sec⁻¹, and shows a very unique microstructure. Comparing Fig. 6b with 6a, we suppose that the large particle seen at the upper left in the photograph is a SiC particle and the particles of relatively uniform size are of SiC/AlN mixture. The small particles are joined together and surround the large SiC particle as a suit of armour. It is difficult

TABLE II Crystallite size (L) and microstrain (ϵ) of shock-treated materials determined by X-ray line-broadening analysis

Material	Velocity							
	Starting		2.0 km sec ⁻¹		2.0 km sec ⁻¹		3.0 km sec ⁻¹	
	L (nm)	ϵ (10 ⁻³)	L (nm)	ϵ (10 ⁻³)	L (nm)	ϵ (10 ⁻³)	L (nm)	ϵ (10 ⁻³)
SiC	32.0	1.04	27.0	4.03	23.0	3.81	59.0	0.66
SiC in SiC/AlN	32.0	1.04	27.0	3.35	21.0	2.42	30.5	1.98
AlN	63.0	2.43	44.0	4.01	37.0	4.93	68.0	0.72
AlN in SiC/AlN	63.0	2.43	65.0	4.10	50.0	7.04	53.5	3.43
AlN in AlN/Al ₂ O ₃	63.0	2.43	63.0	4.96	56.0	7.58	66.0	6.75
AlN (4-3)	—	—	—	—	—	—	64.0	6.37
AlN (5-3)	—	—	—	—	—	—	96.0	4.29
Al ₂ O ₃ in AlN/Al ₂ O ₃	131	0.76	189	0.33	188	1.20	*	*

*Better annealed than the standard material.

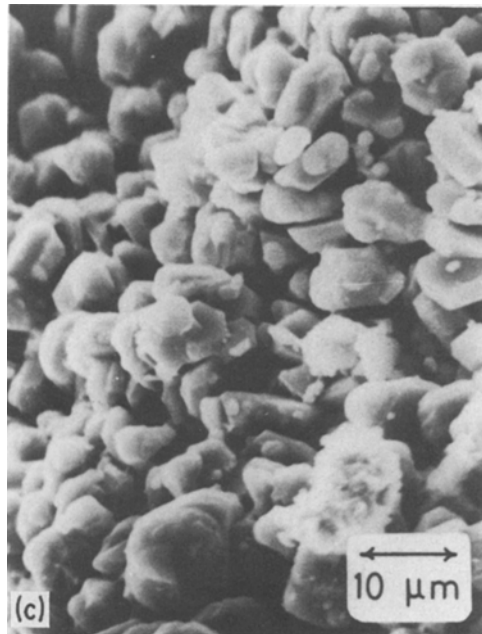
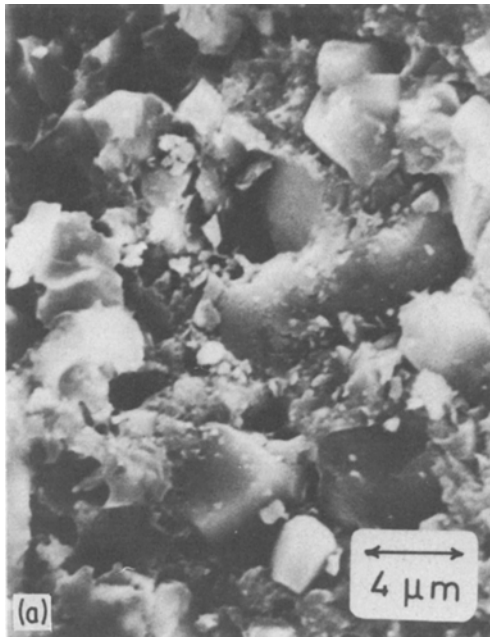


Figure 5 Scanning electron micrographs of the fracture surface of the SiC sample recovered from shock condition. (a), (b) and (c) correspond to impact velocities of 2, 2.3 and 3 km sec⁻¹, respectively.

3.3.3. AlN

Fig. 7 shows scanning electron micrographs for fracture surfaces of the single AlN samples. A photograph of the AlN sample impacted at a velocity of 2 km sec⁻¹ is considerably different from that of SiC, as seen in Figs. 5a and 7a. These homogeneous particles are less than 0.7 μm and consist of stacked layers in each particle. It is obvious that this unique microstructure results from the creation of the unknown new phase rather than from mechanical deformation and fracture. The homogeneous particles are partially joined together and form a secondary cluster, but the bonding seems to be insufficient.

In Fig. 7b, the homogeneous small particles are well joined together with melted material due to the excess thermal energy introduced by the increase of impact velocity. We can see a thin film at the boundary where the secondary particle is probably removed. The size of the secondary particle is similar to that of the SiC/AlN sample (5 to 10 μm) but slightly smaller than that of the single-component SiC sample (less than 5 μm). The thickness of the film is approximately 0.1 μm. It is, however, difficult to identify whether a round trace formed by the film is due to the initial particle or the secondary cluster, because there are AlN particles larger than 10 μm shown in Fig. 1. Moreover, since a shock loading means that the initial powder aggregate jumps into the final state like Fig. 7b, the intermediate process is normally ignored.

At the highest velocity impactation, AlN particles are well joined, and the compact is fractured in the particle, as shown in Fig. 7c. Although the grain boundary is not clear, it does not seem that there are also homogeneous small particles as shown in Fig. 7a. If so, this sample is made by a direct bonding of the

to identify which of the small particles are SiC or AlN. In the small particles, the number of AlN particles must be much larger than that of SiC. The microstrain of the SiC crystal in the SiC/AlN system as a disruptive effect of shock wave, is smaller than that of the single-component SiC sample, but the microstrain of AlN in SiC/AlN is larger than that of the single-component AlN sample. This is attributed to heterogeneous deformation or fracture, which depends on the difference of mechanical or thermal properties between SiC and AlN.

Fig. 6c does not show an epitaxial crystal growth seen in the single-component SiC sample. The microstructure consists of both agglomerated particles of fine grains and continuous parts, which are probably produced by quenching the liquid phase. Changes in the lattice parameters due to the formation of a solid solution of SiC/AlN are not evident from the X-ray diffraction analysis.

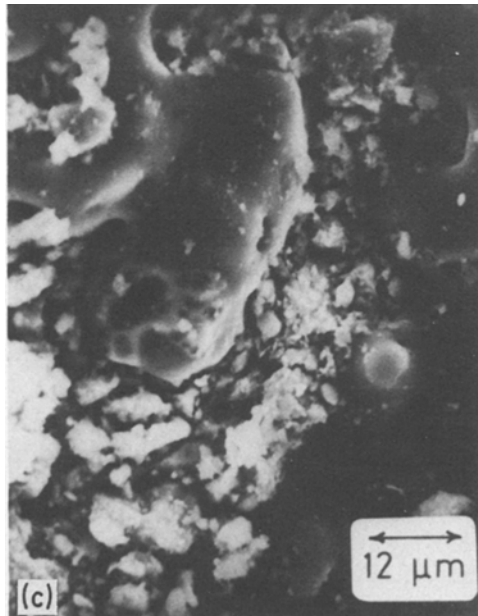
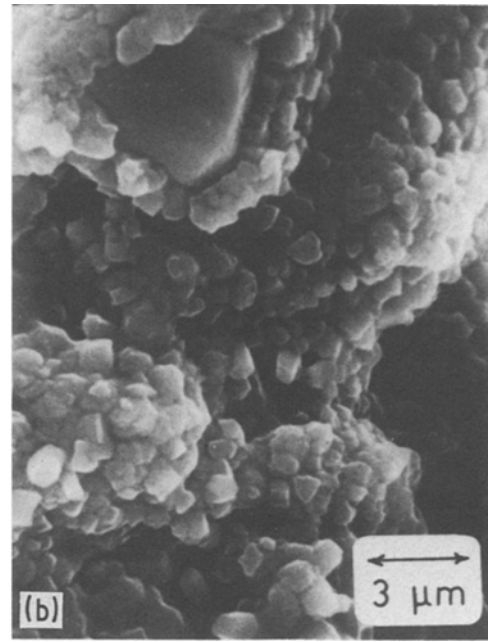


Figure 6 Scanning electron micrographs of the fracture surface of the SiC/AlN mixture sample recovered from shock condition. (a), (b) and (c) correspond to impact velocities of 2, 2.3 and 3 km sec⁻¹, respectively.

AlN with the wurtzite structure, AlN with the unknown new structure, Al₂O₃ with the corundum structure, and ALON with the cubic spinel structure. The complex microstructure results from the phase transition of AlN and from the chemical reaction between AlN and Al₂O₃ accompanying mass transport. We can see some cubic-shaped grains in Fig. 9a which may be of ALON.

At an impact velocity of 2.3 km sec⁻¹, the phase transition of AlN to the unknown new phase and the chemical reaction to ALON seldom occur. The microstructure shown in Fig. 9b is considerably similar to Fig. 7a which is of the single-component AlN sample. We have no interpretation for the micrograph.

4. Discussion

The skin model for powder consolidation mechanism using a shock compression technique is already proposed by some of the authors in order to estimate the heterogeneous shock state which is realized under and after shock loading to the initial powder aggregates.

It is assumed for simplicity that the initial powder aggregates are transformed to the closely packed cubes with a relatively thin skin through a shock front, as shown in Fig. 11 in [2]. Consequently, we consider that the three stages in the shock-compaction process are already achieved in the shock front, in which the powder particles are re-stacked, yielded and/or fractured, and compressed. Jetting from the particle surface into the pore must also be happening in the shock front. Such phenomena depend on shock pressure, initial particle size, initial density, and so on, and result in a shock-front structure with a certain thickness and a consequent time-duration, for example, more than 100 nsec. In any case, we suppose that the

initial particle without undergoing phase transition to the unknown new phase.

Fig. 8 is a photograph of the high purity and high initial density (71%) sample (5-3) impacted at the same velocity as that in Fig. 7c. The microstructure consists of considerably fine grains and a similar amount of pores to that in Fig. 7c. The particle shape of the sample is spherical. In this experiment, shock pressure is three times higher, and shock temperature is approximately 1000° C lower than those for Fig. 7c. The phase transition from wurtzite structure to sodium chloride structure strongly influences the microstructure and the large residual microstrain.

3.3.4. AlN/Al₂O₃

Scanning electron micrographs of fracture surfaces of the AlN/Al₂O₃ mixture sample are shown in Fig. 9. Fig. 9a corresponds to the sample impacted at 2.0 km sec⁻¹. According to the X-ray diffraction analysis, this sample consists of four phases which are

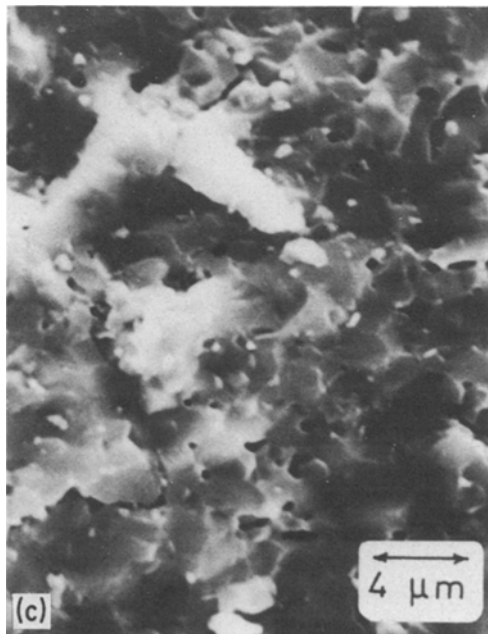
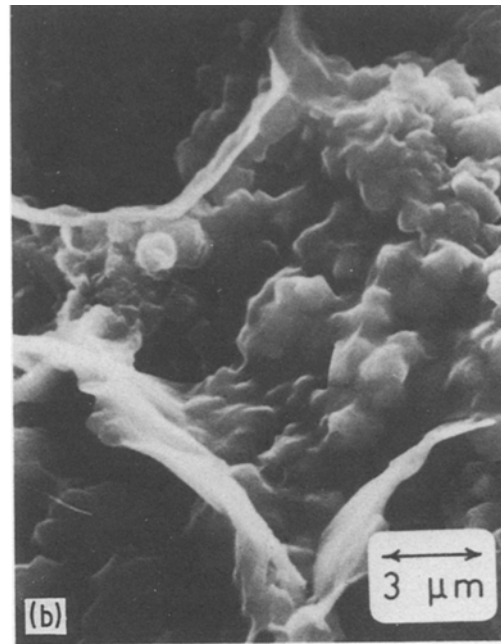
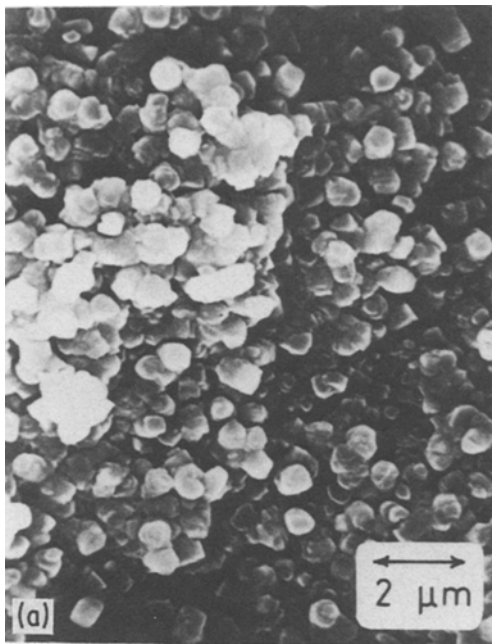


Figure 7 Scanning electron micrographs of the fracture surface of the AlN sample recovered from shock condition. (a), (b) and (c) correspond to impact velocities of 2, 2.3 and 3 km sec⁻¹, respectively.

complicated shock-process mentioned above can be finished in the shock front and then the shock-compressed state, as shown in Fig. 11 in [2], can be achieved after the passage of the shock front. Moreover, since we suppose that the core of the cube is a fragment of the original particle rather than composed of secondarily joined particles, it is likely that the crystal of the core inside of the skin is isentropically compressed or shock-compressed as the full density material without any influences due to the initial porous state. On the other hand, we suppose that the skin includes all the ambiguous effects due to both the initial porous state and the complicated shock process mentioned above. Since mechanical process propagates with a speed of the order of shock-wave velocity, all the materials behind the shock front are in mechanical equilibrium and thus shock pressures must be the same in both the skin and the core. The thermal process is relatively slower than the mechanical

process, and thus it is reasonable that the skin and the core are independent under adiabatic conditions. It is, therefore, possible to divide the total Hugoniot energy for porous material into components for the skin and the core, where the latter is assumed here to be shock-compressed at the crystal density material.

Although the model is of the first order approximation, the idea is fundamental to treat the heterogeneous system, where the mechanical equilibrium can be quickly achieved but the thermal equilibrium takes relatively long time. The skin model predicts that the thermal relaxation phenomena will be critical for a few-micrometre grain in a ceramic compact under and after shock loading. This means that surface melting phenomenon will occur at the size of the grain mentioned above, and then the melted surface will be quenched at the post shock. The previous shock-compaction experiments for SiC fine powder with an average particle size of 0.28 μm did not clearly show the surface melting phenomenon, because the particle size was too small. In the present experiments using larger grain-size SiC powder, some of the shock-compacted samples clearly show the evidence of the surface melting, as shown in Fig. 10. The thickness of the skin, δ , and the corresponding particle size, d , are approximately estimated to be 0.1 and 3 μm, respectively. The value of δ/d becomes 0.03, and then the temperature ratio in the skin to the particle core and that to the equilibrium temperature are approximately 30 and 5 on the figure, respectively. The skin temperature exceeds 10⁴ K. However, since the relaxation time is less than 1 nsec, the skin temperature quickly decreases within the shock front (approximately 0.1 μsec). Therefore, the skin of the particle was melted and then was rapidly quenched via thermal

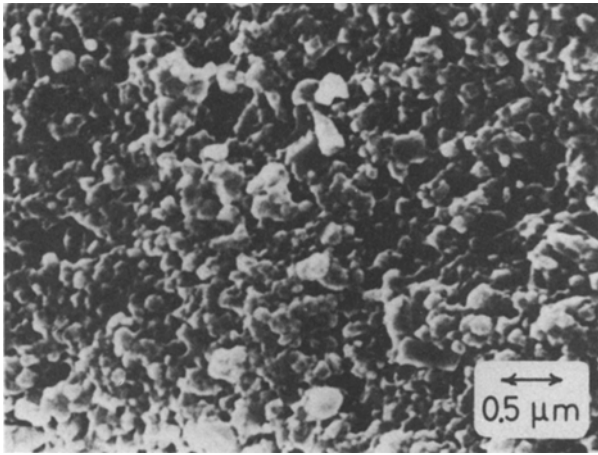


Figure 8 Scanning electron micrograph of the high purity and high initial density (71%) sample impacted at a flyer velocity of 3 km sec^{-1} . Shock pressure is three times higher, and shock temperature is approximately 1000°C lower than those for Fig. 7c.

diffusion process during shock compression. Although the value of δ/d is widely thought to be strongly dependent on the grain size, it is likely that the skin model is strongly supported by the photograph (Fig. 10) obtained here.

In the previous experiments for SiC fine powder, the increase of microstrain (8 to 9×10^{-3}) was more remarkable rather than the crystallite size reduction (60 to 70 nm), on the shock condition similar to that in the present work. On the other hand, the present experiments for SiC coarser powder result in a smaller crystallite size (23 to 27 nm) and a smaller increase of microstrain (3.8 to 4.0×10^{-3}). This may be dependent on the difference of starting powders, but it is also possible to reasonably interpret this result as follows.

According to the skin model, the core temperature in a coarser powder particle is kept at a low temperature for a time which is longer than either the time in which the shock pressure rises up to the equilibrium value or the core temperature in a fine powder particle would rise up to the equilibrium value due to the thermal diffusion process. Therefore, since the coarser particle is strained at lower temperature, the crystals are fractured as easily as a sufficiently brittle material so that the deformation energy introduced by shock compression is absorbed as crystallite size reduction. On the other hand, such fine powder particle with a submicrometre diameter can approach an equilibrium temperature much higher than the initial core temperature, the crystals are plastically deformed as easily as a more ductile powder than the above. Thus, the increase of microstrain for a fine powder is greater than that obtained here. The value of Vicker's microhardness obtained here, which is lower than those in the previous experiments, is caused by the fact that the crystal includes a great number of macro- and microcracks due to the above mechanism. If we consider this process as a preconditioning prior to the subsequent normal sintering process, a better result will be attained when the size of the initial particle is larger. Further experiments and evaluations will be necessary in order to determine what size of the particle is optimum. AlN is reported as a slightly ductile ceramic material in comparison with the other non-oxide ceramics because of the ability to sustain a large microstrain [17]. The largest microstrain reported in 3×10^{-3} which is saturated in the pressure region from 10 to 30 GPa . The maximum microstrain obtained here is 7.6×10^{-3} which is two and a half times larger than the above. This is influenced by

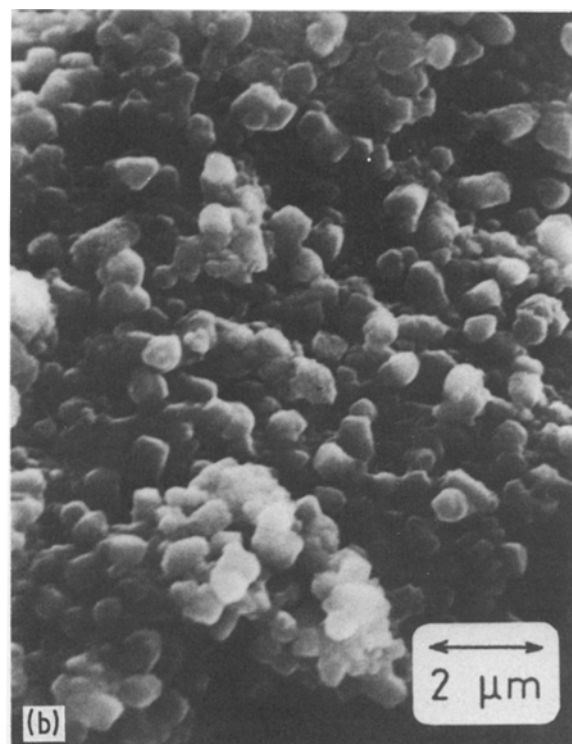
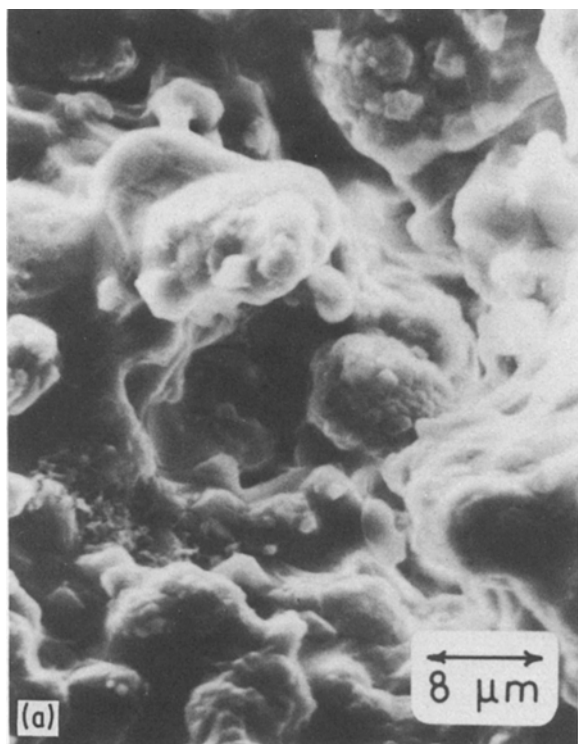


Figure 9 Scanning electron micrograph of the fracture surface of the AlN/Al₂O₃ mixture sample recovered from shock condition. (a) and (b) correspond to impact velocities of 2 and 2.3 km sec^{-1} , respectively.

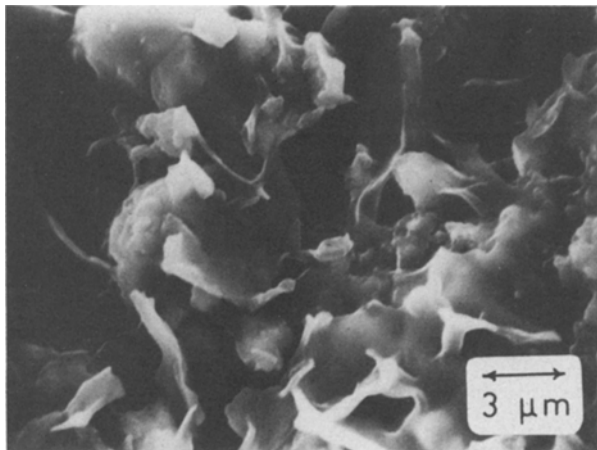


Figure 10 Scanning electron micrograph of the fracture surface of the SiC sample impacted at a flyer velocity of 2.3 km sec^{-1} . This is for another part of the shock-compacted sample shown in Fig. 5b. The micrograph shows evidence of the surface melting and provides support for the skin model.

the phase transition to the unknown phase and the chemical reaction with the other species, as described later.

High-pressure phase transition in AlN has been pointed out by some of the authors via an equation of state experiment and electrical conductivity measurements using a shock compression technique. It is known that wurtzite (hexagonal ZnS) transforms to sphalerite (cubic ZnS) below 4.5 GPa [18] and that the sphalerite undergoes transition to sodium chloride structure at $15.0 \pm 0.5 \text{ GPa}$ [19, 20]. The transition for AlN occurring at approximately 20 GPa is inferred as the structural transition from the wurtzite structure to the sodium chloride structure by analogy. In only two shots, shock pressure exceeds the phase transition pressure, but the samples recovered do not include the high-pressure phase modification. Although X-ray diffraction experiment for the samples shows only wurtzite type AlN, the scanning electron micrograph (Fig. 8) shows considerably uniform and fine particles (less than $0.1 \mu\text{m}$), while the starting powder consists of particles of a size of a few micrometres. There would be some indirect evidence for transition as the fine uniform particles are thought to originate from nucleation of the high-pressure phase during shock compression and/or the nucleation of the wurtzite phase from the high pressure one in the post-shock state.

Vereshchagin *et al.* [4] have already reported the unknown phase of AlN, which showed additional strong X-ray diffraction lines at the lower angles as in the present work. The phase of AlN was produced under shock compression, static high pressure (30 GPa) with strong shear stress at ambient temperature, or a static condition of 5.5 GPa pressure and 1000°C heating [4]. The density of specimens including much of the AlN new phase was little different from that of the wurtzite type AlN. Although the unknown phase of AlN was expected to be of sphalerite structure by analogy in ZnS, their careful determinations of the X-ray diffraction results did not confirm the formation of the sphalerite (cubic) modification.

The thermal stability of the tetrahedral structures of the wurtzite and sphalerite types are discussed as based on crystal structural and physical data of AlN, BeO, ZnS, and SiC [21]. A consideration of ionic configuration energies of these compounds leads to a conclusion that the wurtzite type structure is stable at least in low temperature region for all of these binary compounds. If vibrational entropy is taken into account for the energy, the stable form at higher temperature tends to be of the sphalerite type, especially for those in which the difference of electronegativity of the component elements is less than around unity. The situation is similar in the system of wurtzite type BN and sphalerite type BN [22, 23]. Therefore, another type of contribution to the structural stability should be introduced into the discussion for the unknown new phase.

As shown in Fig. 4, the strongest peaks for the unknown phase, which are located at 27° and 2θ , and are two times larger than the strongest peak for the wurtzite type AlN (33.2° in 2θ) in the AlN/Al₂O₃ impacted at 2 km sec^{-1} . This means that the amount of the new phase of AlN produced in AlN/Al₂O₃ system is four times larger than that in the single-component AlN sample, as referred to the strongest peak of AlN. As the increase of impact velocity approximately corresponds to the increase of shock temperature, it is clear that the new phase creation occurs more easily at low temperature, probably less than 1400 K, and that an inverse transition to the original phase occurs at high temperature. This suggests that shear stresses rather than pressure are dominant to the transition.

Although similar static high-pressure experiments to those of Vereshchagin *et al.* were carried out for the high-purity AlN specimen, the unknown new phase was not detected. Considering that the unknown phase was not produced in either the SiC/AlN sample or the high-purity AlN sample, but was produced in great quantity in the AlN/Al₂O₃ sample rather than in the single-component AlN, we conclude that the existence of a small amount of oxygen is the most important factor for creation of the new phase. The d spacings for the strongest peaks are 0.3298 and 0.2695 nm, respectively. One of the polytypes such as α -SiC due to stacking faults [12] cannot be expected as the unknown phase modification, because the former spacing is too large and is not an integral multiple of the normal spacing. If we speculate the new modification by analogy in IV and III–V group compounds, the d spacing corresponds to the C plane of the crystal structure like graphite or low-pressure phase of BN.

It is surprising that mass transport and consequent reconstructive chemical reaction occur in a short period such as shock loading. It is recognized that the heterogeneous deformation for brittle materials strongly affects reconstructive phase transition and dissociation reaction, for example, those in anorthite and forsterite to an assemblage of MgO plus MgSiO₃ perovskite [24, 25]. Although the pressure- and temperature-release process from the shock-compressed state to the ambient condition is not well characterized, it is clear that extremely high temperature and

the effect of mechanical mixing due to a stress gradient are necessary for such short-time chemical reactions to occur in a shock process. The skin model is found consistent with the reaction because of the existence of such an extremely high temperature. Materials at the high temperature must melt or vaporize and then are mixed by the consequent potential gradients. Since thermal diffusion process from the skin to the core also is realized in the extreme temperature gradients, the recrystallization process must be accelerated.

Investigations on phase stability in the system SiC/AlN have been carried out by several authors [10, 11, 26], and show the formation of solid solution at high temperature, which is obeyed by the Vegard's law. However, we could not detect solid solution of the SiC/AlN system within experimental accuracy in these experiments. The α -phase SiC, which is of similar symmetry to that of AlN, were used in those studies. Since a kind of phase transition from β - to α -phase has to be accompanied, the reaction would not occur easily. At an impact velocity of 2.3 km sec^{-1} , the (1 1 1) line for β -SiC and the (0 0 2) for AlN are combined. The line (3 1 1) for β -SiC and the (1 1 2) for AlN are also combined at a velocity except for 2.0 km sec^{-1} . They suggest that a partial reaction occurs at the impact velocities, and that the large increase of reactivity in the mixture sample will be observed when the sample is heat-treated by a traditional sintering process. As mentioned before, the microstrain of SiC crystal in the SiC/AlN system has a disruptive effect on shock wave and is smaller than that of the single-component SiC sample at an impact velocity except for 3 km sec^{-1} , but the microstrain of AlN in SiC/AlN is larger than that of the single-component AlN sample. This means that SiC atoms undergoing the disruptive effect are soluble in the AlN lattice with a hexagonal symmetry and then distort the crystal lattice. The larger microstrain than any other reported for AlN [17] is influenced by the above chemical reaction. There has been a similar example observed in $\text{Si}_3\text{N}_4/\text{Y}_2\text{O}_3$ system [27]. The shock-treated powders of $\text{Si}_3\text{N}_4/\text{Y}_2\text{O}_3$ mixture are not drastically changed in the X-ray diffraction profile from the starting powder, but densification and solubility of Y_2O_3 into the lattice are remarkable in hot isostatic pressing.

According to the skin model estimation and scanning electron micrographs, the initial particle size of AlN and SiC powder is too large to complete the chemical reaction. On the other hand, in the AlN/ Al_2O_3 system, the particle size of Al_2O_3 was $0.3 \mu\text{m}$ so that ALON was produced in a shock process. Although the chemical reaction of AlN and Al_2O_3 for ALON reasonably depends on the average shock temperature, it is difficult to discuss quantitatively the amount of ALON produced, because peaks of ALON are broadened and superimposed by the others. AlN particles are still too large compared to Al_2O_3 particles, and the creation of the unknown phase makes the chemical reaction process complicated. It is concluded that we should select the particle size small enough to obtain the thermodynamical equilibrium in a shock rising front. In order to decide the optimum

particle size for shock-induced chemical reaction, the figure for relaxation time against thickness of the skin shown in the previous report [2] is available by substituting particle radius for thickness. The particle size of a submicrometre diameter will be essential in the experimental arrangements used here.

A theory for the shock-wave consolidation of powders proposed by Schwarz *et al.* [28] is available to predict the regimes of shock pressure and shock duration expected to yield fully densified metallic compacts of near optimum strength. The model gives an upper bound to the amount of melt. The condition that the melt between particles must exceed a critical thickness and must be solidified within the duration of the shocked state leads to necessary conditions for the pressure and duration. Although one of the important parameters in the theory strongly depends on the initial particle size, the theory is available for metallic powders because the metallic powders are easily deformed rather than fractured under shock loading. Morris [29] examined the microstructures of a range of metallic powder compacts obtained by dynamic or shock-wave compaction in an attempt to elucidate the processes leading to bonding. The conclusions, which are similar to the above theory, are based on the strain localization around the initial particle exteriors.

On the other hand, in one way that the initial particles are pulverized, the resultant particle size and its distribution are essentially important. The usual ceramic powders with a large particle size such as $300 \mu\text{m}$ are pulverized into particles of a few micrometres diameter, e.g. alumina in [16]. The ceramic powders with an initial particle size of several micrometres are also pulverized and result in a wide range of particle-size distribution from submicrometres to a few micrometres, as obtained here. Since the skin model is based on the resultant particle size, the model is useful for brittle materials.

There are, however, some phenomena dependent on the initial particle size for ceramic powders. The first, the final particle size and its distribution under and after shock loading, depends on the initial state such as particle size and porosity. The second, the number of nucleations for recrystallization, depends on the initial particle size or the number of the particles, as shown here. They are remarkable in the case of the initial particle size of more than a few micrometres. The third, the size of the cluster which is formed by particle aggregation, also depends on the initial particle size. The initial stage in the traditional sintering process is identified as a formation of the cluster, which is remarkably observed in the case of fine powders of less than $1 \mu\text{m}$. The phenomenon similar to this stage is also observed in these shock consolidation processes for fine SiC or AlN powder, where the latter accompanies transformation to the unknown phase and results in uniform fine particles.

In conclusion, it may strongly affect this dynamic process for ceramic powders whether the initial particle size exceeds $1 \mu\text{m}$ or not. That the initial particle size is less than $1 \mu\text{m}$ is essentially important for ceramic powder to be consolidated, for the purpose of yielding fully densified compacts of near optimum

strength and achieving chemical reaction with mass transport. The reasons are that the mass transport process cannot cover large distances and that the rapid increase of core temperature promotes plastic deformation and mass transport. This is strongly related to the shock-rise time rather than the shock duration. It is, therefore, necessary to study the relationship between the initial size, final particle size, and characteristics in shock-wave propagation via *in situ* observations.

References

1. V. D. LINSE, Dynamic Compaction of Metal and Ceramic Powders, Report of the Committee on Dynamic Compaction of Metal and Ceramic Powders, edited by National Materials Advisory Board, NMAB-394 (National Academy Press, Washington, DG, 1983) p. 1.
2. K. KONDO, S. SOGA, A. SAWAOKA and M. ARAKI, *J. Mater. Sci.* in press.
3. K. KONDO, A. SAWAOKA, K. SATO and M. ANDO, "Shock Waves in Condensed Matter", edited by W. J. Nellis, L. Seaman and R. A. Graham, AIP Conference Proceedings 78 (American Institute of Physics, New York, NY, 1982), p. 325.
4. L. F. VERESHCHAGIN, G. A. ADADUROV, O. N. BREUSOV, K. P. BURDINA, L. N. BURENKOVA, A. N. DREMIN, E. V. ZUBOVA and A. I. RAGACHEVA, *Sov. Phys. Doklady* **13** (1969) 896.
5. W. A. RACHINGER, *J. Sci. Instrum.* **25** (1948) 254.
6. H. P. KLUG and L. E. ALEXANDER, "X-ray Diffraction Procedures" (Wiley, New York, 1974) p. 618.
7. A. SAWAOKA, K. KONDO and T. AKASHI, *Report Res. Lab. Eng. Mat. Tokyo Inst. Tech.* **4** (1979) p. 109.
8. R. G. McQUEEN, S. P. MARSH, J. W. TAYLOR, J. N. FRITZ and W. J. CARTER, "High-Velocity Impact Phenomena", edited by R. Kinslow (Academic Press, New York, 1970) p. 244.
9. P. E. MUNSON, R. R. BOADE and K. W. SCHULER, *J. Appl. Phys.* **49** (1978) 4797.
10. W. RANFANIELLO, M. R. PLICHTA and A. V. VIRKAR, *J. Amer. Ceram. Soc.* **66** (1983) 272.
11. M. SHIMADA, K. SASAKI and M. KOIZUMI, Proceedings of the International Symposium on Ceramic Components for Engine, Hakone (1983) in press.
12. T. SAKAI, *J. Ceram. Soc. Jpn* **86** (1978) 125.
13. J. W. McCAULEY and N. D. CORBIN, *J. Amer. Ceram. Soc.* **62** (1979) 476.
14. D. TURPIN-LAUNAY, F. THEVENOT, F. DELVOYE and P. BOCH, "Ceramic Powders", edited by P. Vincenzini (Elsevier, Amsterdam, 1983) p. 891.
15. O. R. BERGMANN and J. BARRINGTON, *J. Amer. Ceram. Soc.* **49** (1966) 502.
16. R. A. PRÜEMMER and G. ZIEGLER, *Powder Met. Int.* **9** (1977) 11.
17. B. MOROSIN and R. A. GRAHAM, "Defect Properties and Processing of High-Technology Nonmetallic Materials", Materials Research Society Symposia Proceedings 24, edited by L. H. Crawford Jr, Y. Chen and W. A. Sibley (Elsevier, New York, 1984) p. 335.
18. C. F. CLINE and D. R. STEPHENS, *J. Appl. Phys.* **36** (1965) 2869.
19. G. A. SAMARA and H. G. DRICKAMER, *J. Phys. Chem. Solids* **23** (1962) 457.
20. S. C. YU, I. L. SPAIN and E. F. SKELTON, *Solid State Commun.* **25** (1978) 49.
21. Y. INOMATA, *J. Ceram. Soc. Jpn* **78** (1970) 365.
22. F. R. CORGAN and F. P. BUNDY, *J. Chem. Phys.* **63** (1975) 3812.
23. T. AKASHI, A. SAWAOKA and S. SAITO, *J. Amer. Ceram. Soc.* **61** (1978) 245.
24. Y. SYONO, T. GOTO, Y. NAKAGAWA and M. KITAMURA, "High Pressure Research: Application in Geophysics" (Academic, New York, 1977) p. 477.
25. Y. SHONO, T. GOTO, H. TAKEI, M. TOKONAMI and K. NOBUGAI, *Science* **214** (1981) 177.
26. W. RAFANIELLO, K. CHO and A. V. VIRKAR, *J. Mater. Sci.* **16** (1981) 3479.
27. S. SOMIYA, M. YOSHIMURA, S. FUJIWARA, K. KONDO, A. SAWAOKA, T. HATTORI, J. MOHRI and M. ARAKI, *J. Amer. Ceram. Soc.* **67** (1984) C-51.
28. R. B. SCHWARZ, P. KASIRAJ, T. VREELAND Jr and T. J. AHRENS, *Acta Metall.* **32** (1984) 1243.
29. D. G. MORRIS, *Mater. Sci. Eng.* **57** (1983) 187.

Received 4 March
and accepted 30 May 1985